PAVEL, N. V., QUAGLIATA, C. & SCARCELLI, N. (1976). *Z. Kristallogr.* **144**, 64–75. Dort weitere Literatur.
PERTSIN, A. J., IVANOV, YU. P. & KITAIGORODSKY, A. I. (1981). *Acta Cryst.* A**37**, 908–913.
TAYLOR, J. C. & WILSON, P. W. (1974). *Acta Cryst.* B**30**, 1481–1484.
TAYLOR, J. C. & WILSON, P. W. (1975). *J. Solid State Chem.* **14**, 378–382.
TAYLOR, J. C., WILSON, P. W. & KELLY, J. W. (1973). *Acta Cryst.* B**29**, 7–12.
WILLIAMS, D. E. & HOUPT, D. J. (1986). *Acta Cryst.* B**42**, 286–295. Dort weitere Literatur.
WILLING, W. (1986). *GITTEN*. Programm zur Berechnung von Gitterenergien in Molekülkristallen. Univ. Marburg, Bundesrepublik Deutschland.
WILLING, W. & MÜLLER, U. (1987). *Acta Cryst.* C**43**, 1425–1426.

Acta Cryst. (1988). B**44**, 6–11

Hendricks–Teller Analysis of Stacking-Fault-Broadened Profiles in $C_{24}Rb$

BY C. THOMPSON,* M. E. MISENHEIMER† AND S. C. MOSS

Department of Physics, The University of Houston, Houston, TX 77004, *USA*

(*Received* 26 *June* 1987; *accepted* 10 *September* 1987)

Abstract

An X-ray diffraction profile analysis using a Hendricks–Teller model with a single second-neighbor interplanar correlation parameter gives good agreement with experimental diffraction scans on a highly-oriented pyrolytic graphite (HOPG) sample of $C_{24}Rb$ where the rubidium is in a disordered or liquid state. The stacking-fault probability is 0·20. It is noted that for crystals with a large mosaic distribution the resolution of low-index profiles is considerably degraded when the scan direction is parallel to the mosaic spread. The profile fitting permitted an accurate determination of the alkali contribution to the host Bragg peaks in the highly faulted material.

Introduction

The graphite structure consists of a layered sequence of strongly bonded hexagonal-net planes of carbon atoms separated by a van der Waals gap of 3·35 Å. These planes are stacked in a sequence *ABAB*... in which the atoms in the *B* layer are shifted with respect to those in the *A* layer by an amount: $2/3\ \mathbf{a}_1 + 1/3\ \mathbf{a}_2$, where $\mathbf{a}_1$ and $\mathbf{a}_2$ are the unit-cell basal-plane translation vectors, and $|\mathbf{a}_1| = |\mathbf{a}_2| = 2{\cdot}46$ Å. The unit cell of this structure contains four atoms located at (0,0,0) $(0,0,\frac{1}{2})$, $(\frac{1}{3},\frac{2}{3},0)$, $(\frac{2}{3},\frac{1}{3},\frac{1}{2})$ (Kelly & Groves, 1970), and the resulting diffraction pattern consists of two types of *hk.l* reflections: (1) *l* even, all *h*, *k* permitted; (2) *l* odd, only $h + 2k = 3m \pm 1$ (m = integer) permitted.

Because the interlayer bonding is weak there can be extensive faulting in graphite. In particular, in highly oriented pyrolytic graphite (HOPG) one may encounter a quite measurable density of stacking faults that arise during preparation (Moore, 1973). These faults consist mainly of shifts in the layer sequence noted above and may take the form *ABABCBCBC*..., for example, in which a packet of *ABC* is inserted in the *AB* sequence converting it to the equivalent *BCBCBC*... sequence. The insertion of a piece of *ABC* into *ABAB* can be thought of as analogous to the introduction of an f.c.c. packet into h.c.p. where f.c.c. and h.c.p. refer to the face-centered-cubic and hexagonal-close-packed sequences. The shift of the *C* layer with respect to *B* is given by an additional $2/3\ \mathbf{a}_1 + 1/3\ \mathbf{a}_2$.

Upon intercalation of the graphite with the alkali metals to stage 2, as in $C_{24}Rb$, the stacking sequence is converted to *A/AB/BC/CA/A*... (Parry, Nixon, Lester & Levene, 1969; Parry & Nixon, 1967; Nixon & Parry, 1968) in which *A* refers, as above, to graphite and the slashed line (/) refers to a layer of disordered or liquid-like alkali metal. The stage index refers to the number of carbon layers separating intercalate layers. In this case, it is convenient to consider a sandwich layer of graphite–alkali–graphite as a single unit. The graphite layers bounding the alkali are positioned directly over each other. The normal sequence for stage 2 is then f.c.c. and faults consist of h.c.p. material inserted, nominally at random, in this f.c.c. sequence.

If we calculate the structure factor for the f.c.c.-sequenced compound [composed of three layer units and actually of rhombohedral symmetry ($R\bar{3}m$) rather than cubic] we obtain the following selection rules: (1) $l = 3m$, only $h + 2k = 3n$ permitted (m, n = integers); (2) $l = 3m \pm 1$, only $h + 2k = 3n \pm 1$ permitted. The first set for $l = 3m$ gives the same reflections that one encounters at $l = 2m$ for the h.c.p. sequence. These reflections are therefore not affected by this type of faulting. The reflections of the second set appear at

* Present address: IBM Thomas J. Watson Research Center, PO Box 218, Yorktown Heights, NY 10598, USA.
† Present address: Tracor Northern, 2551 W. Beltline, Middleton, WI 53562, USA.

0108-7681/88/010006-06$03.00

different values of l in the two cases, naturally adjusted to account for the fact that the c-axis lattice parameter, $c_{\text{f.c.c.}} = (3/2)\ c_{\text{h.c.p.}}$, and show directly the effect of faulting through a smearing and shifting of the intensity along l between the positions associated with the separate cases. Reflections such as 00.l, 11.l, 30.l and 22.l are unaffected whereas the profiles of the class 10.l and 21.l show the faulting clearly and are examined in detail here.

Stacking-fault models

Two basic methods of deriving quantitative stacking-fault information from X-ray diffraction profiles have been developed and refined by many workers (Warren, 1969; Hendricks & Teller, 1942; Kakinoki & Komura, 1965). The first, as described by Warren (1969) for the case of deformed metals, considers two classes of stacking faults, deformation and twin, and assumes that each is independent of the other and randomly distributed with respective parameters α and β. In the f.c.c. sequence, a twin fault with probability β follows the scheme

$$ABCABCAB\underline{A}CBACB,$$

while a deformation fault, with probability α follows the scheme

$$ABCABCAB\underline{A}BCABC$$

where, in both cases, the fault layer is underlined. These two differ in which of the two possible alternate layers follow the fault layer ($\underline{A}B$ or $\underline{A}C$) since the f.c.c. sequence is regained after this point. It is clear that the deformation fault is simply two consecutive twin faults. Thus α and β are not independent, and $\alpha = \beta^2$. The fact that this method has been successfully used to study stacking faults in cold-worked metals means that the correlated (double) twin fault which restores the original f.c.c. sequence is appropriate to the deformation of an initially f.c.c. metal.

A more general method for calculating the diffraction pattern of a layered structure incorporating various types of one-dimensional (1D) disorder, including stacking faults and layer spacing variations, was developed by Hendricks & Teller (1942) and extended by Kakinoki & Komura (1965). The Hendricks & Teller (1942) calculations were originally applied to clays, in which hydration leads to a variation in layer spacing, and their treatment has recently been used to interpret the 00.l diffraction profiles in mixed-stage graphite intercalation compounds (GIC's) (Misenheimer & Zabel, 1985; Huster, Heiney, Cajipe & Fischer, 1987). Stacking-fault profiles along 10.l in stage 2 alkali-metal GIC's have also been examined by Hastings, Ellenson & Fischer (1979), Rousseaux, Tchoubar, Tchoubar, Guerard, Lagrange, Herold & Moret (1983), and Nishitani, Suda & Suematsu (1986). Hendricks & Teller (1942) also applied their general formulation to h.c.p/f.c.c. stacking faults in graphite. If one neglects correlations among faults, an l-dependent profile can be calculated using a single free parameter referred to here as x_{HT}. The Hendricks–Teller method is based on the fact that the difference between h.c.p. and f.c.c. stacking sequences appears only at the next-nearest-neighbor, rather than the nearest-neighbor layer, *i.e. ABA versus ABC*. Therefore, rather than consider layers of carbon planes, this extension of Hendricks & Teller (1942) treats pairs of layers.

If we pick a pair of layers we can, without loss of generality, label them (AB). Since a pure graphite layer will not be stacked directly over itself, the next pair of layers can be one of four possibilities, (AB), (AC), (CB) and (CA). The first choice results in h.c.p. stacking while the last gives f.c.c stacking. If p is the probability that the second pair is stacked (AB), then x_{HT} is defined such that $x_{\text{HT}}p$ is the probability that the second pair is stacked (AC). If all three layer types (A,B,C) occur with equal frequency, $x_{\text{HT}}p$ is also the probability that the second pair is stacked (CB). Furthermore, the probability that the second pair is stacked (CA) is $x_{\text{HT}}^2 p$. Since one of the four possibilities must occur,

$$p + x_{\text{HT}}p + x_{\text{HT}}p + x_{\text{HT}}^2 p = 1; \qquad (1)$$

thus

$$p = 1/(1 + x_{\text{HT}})^2. \qquad (2)$$

Therefore x_{HT} is the only parameter needed to describe the probability of any of the four possibilities.

The correspondence between x_{HT} and the stacking-fault probability, $\alpha_{\text{f.c.c.}}$, is given as follows. The probability that a pair of layers, or graphite–metal–graphite sandwiches, in a sequence (AB) is followed by a second pair in the sequence (CA), *i.e.* (AB)(CA), is $x_{\text{HT}}^2 p$. From (2) this can be written as $(x_{\text{HT}})^2/(1 + x_{\text{HT}})^2$. $ABCA$ is f.c.c. stacking. If $\alpha_{\text{f.c.c.}}$ is the probability that a fault occurs in this sequence, then the probability that the (CA) pair follows the (AB) pair is $(1 - \alpha_{\text{f.c.c.}})^2$.

$$1 - \alpha_{\text{f.c.c.}} = x_{\text{HT}}/(1 + x_{\text{HT}})$$

$$\alpha_{\text{f.c.c.}} = 1/(1 + x_{\text{HT}}). \qquad (3)$$

Note that $\alpha_{\text{f.c.c.}}$ is β in Warren's (1969) notation.

In the present case, we must consider a unit-cell stacking of $A/AB/BC/CA/A\ldots$ in which the (AB) graphite pair considered above is replaced by ($A/AB/B$). We will therefore be concerned with the actual structure factor of a given sandwich of graphite–alkali–graphite. The profile fits and analysis in this paper are part of a larger experimental program on anomalous scattering from the disordered $C_{24}Rb$ which uses synchrotron radiation at energies near the rubidium K absorption edge, the principal purpose of which has been to determine the enhancement of graphite Bragg peaks due to a Bragg-like contribution

from the host-modulated alkali intercalate (Thompson, Moss, Reiter & Misenheimer, 1985; Thompson, 1987; Thompson & Moss, 1987). A profile analysis is necessary for a determination of this modulated-liquid contribution to the sandwich-layer structure factor of the fault-broadened peaks. A full description of the anomalous-scattering experiment is given in Thompson & Moss (1987).

Experimental

The scans described here were taken at room temperature at the Stanford Synchrotron Radiation Laboratory (SSRL) on an HOPG sample of $C_{24}Rb$, which was sealed in helium in an aluminium can and was provided by H. Zabel. The energies were chosen in general near the rubidium absorption edge at 15·203 keV (0·815 Å) for purposes of anomalous scattering. The energy used for the profiles discussed here was 14·700 keV (0·84 Å). The morphology of HOPG is polycrystalline with the a axis randomly oriented from grain to grain but with c axes of different grains aligned perpendicular to the surface of the flat-plate geometry of the specimens (Moore, 1973). The mosaic spread of the c axis in the intercalated specimen was approximately 2·5°. The sample was approximately 10 × 10 × 0·5 mm. The c-axis dimension was 27·12 Å and the a-axis dimension was 2·47 Å. The stacking-fault-broadened profiles were corrected for absorption in the asymmetric transmission geometry for a flat plate (Cullity, 1956), and for the geometrical correction given by

$$\lambda^2/[\cos(\theta - \alpha)\sin\theta], \qquad (4)$$

where the $\sin\theta$ term takes account of the resolution element perpendicular to the scan direction when the collimation in this resolution element is smaller than the mosaic spread (Axe & Hastings, 1983), and the remainder of the geometrical function is calculated using the Buerger (1960) treatment for scans at constant q_l intervals. A polarization correction was not applied because the synchrotron beam is over 98% polarized perpendicular to the diffraction vectors used in the experimental geometry.

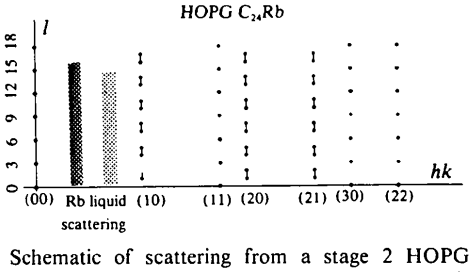

Fig. 1. Schematic of scattering from a stage 2 HOPG alkali-metal–graphite intercalation compound. The stacking-fault-broadened peaks are indicated by lines joining the reflections.

Fig. 1 illustrates schematically the Bragg peaks observed in the diffraction patterns appropriate to HOPG of the stage 2 alkali-metal GIC's. Note that the selection rule $h + 2k \pm l = 3n$ is followed. The two-dimensional disordered alkali-metal layers give rise at room temperature to strong diffuse scattering seen between the 10.0 reflection and the origin (Parry *et al.*, 1969; Clarke, Caswell, Solin & Horn, 1979; Mori, Moss & Jan, 1983; Ohshima, Moss & Clarke, 1985). Although the sequence of layers along **c*** is ordered, the 00.l peaks are not affected by the in-plane alkali-metal layer correlations. Several crystallographic parameters necessary to the profile analysis may therefore be unambiguously determined for the sample by analysis of the 00.l intensities. The deviation from exact stoichiometry (x), the c-axis components of the rubidium and carbon Debye–Waller factors (B^l_{Rb},B^l_C), and the ratio of the sandwich thickness to unit-cell c-axis dimension (c_1) were determined in this manner. The symbol x enters into the stoichiometry as $C_{24/x}Rb$. The 00.l structure factor per sandwich is given by

$$F_{00.l}/3 = 4f_C \exp(-M^l_C)\cos(\pi l c_1) + (x/6)f_{Rb}\exp(-M^l_{Rb}). \qquad (5)$$

The quantity M_y equals $B_y(q_l^2/16\pi^2)$, where y signifies carbon or rubidium. For our wavelength at an energy approximately 500 eV below the rubidium absorption edge, tabulated values of calculated dispersion corrections (Sasaki, 1984) were assumed to be sufficiently accurate. At the other energies studied (15·188, 15·198 keV) self-consistent dispersion corrections were experimentally determined.

Results and analysis

Figs. 2 and 3 show fault-broadened profiles along 10.l and 21.l respectively. The 11.l profile shown in Fig. 4 is not affected by faulting and can be used to assess the instrumental contribution to Figs. 2 and 3. This will be significant because of the way that the resolution volume intersects the mosaic spread in our l scans.

The broadened profiles were fitted by the Hendricks–Teller model with a single nearest-neighbor interplanar correlation parameter x_{HT}.

$$\mathscr{I}(x_{HT}, \varphi) = \frac{(1 + x_{HT})^2}{(4 - 3x_{HT}^2)^{1/2}} \times \left\{ \frac{(4 - 3x_{HT}^2)^{1/2}(2 - \cos\varphi/2) + 3ix_{HT}\sin\varphi/2 - 2 + 4\cos\varphi/2}{2(1 + x_{HT})^2 - [2 - x_{HT}^2 - x_{HT}(4 - 3x_{HT}^2)^{1/2}]\exp(-i\varphi)} + \frac{(4 - 3x_{HT}^2)^{1/2}(2 - \cos\varphi/2) - 3ix_{HT}\sin\varphi/2 + 2 - 4\cos\varphi/2}{2(1 + x_{HT})^2 - [2 - x_{HT}^2 + x_{HT}(4 - 3x_{HT}^2)^{1/2}]\exp(-i\varphi)} \right\} + \text{complex conjugate} - (2 - \cos\varphi/2). \qquad (6)$$

The variable φ is equal to $2\pi l/3$. Equation (6) is equation (34) from Hendricks & Teller (1942), in which the single variable x_{HT} has the value of infinity for a perfect f.c.c. stacking sequence, and zero for perfect h.c.p.

While the stamps of the profiles in Figs. 2 and 3 are determined by the fault probability, the calculation of the relative intensity requires a knowledge of the structure factor per stacking unit which in this system is a graphite–metal–graphite sandwich. This enters into the fitting procedure as a function $|F_{hk.l}|^2$ which is multiplied by the Hendricks–Teller profile function $\mathscr{H}$ in (6). A constant normalization factor is also used to scale the total calculated profile to the experimental profile:

$$I_{hk.l} = N\mathscr{H}(x_{HT}, \varphi)|F_{hk.l}|^2. \quad (7)$$

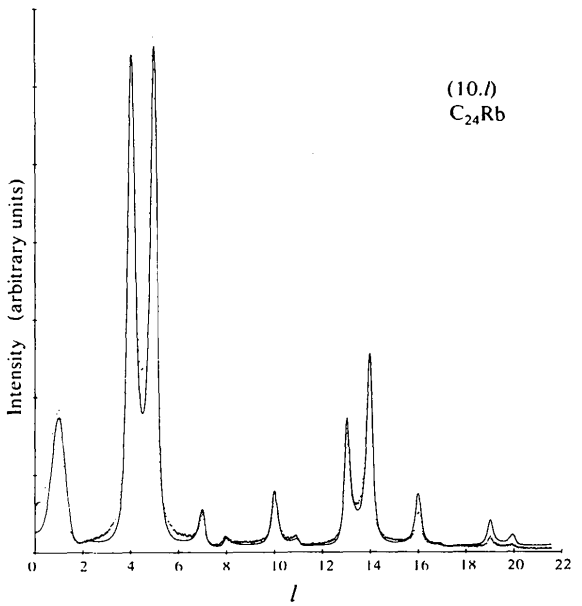

Fig. 2. (10.*l*) experimental profile and Hendricks–Teller fit with a projection convolution applied whose width has been calculated with equation (10) and the values indicated in the text. The solid line is the calculated fit. The stacking-fault probability was fixed at 0·20.

The rubidium contribution to the graphite Bragg peaks other than 00.*l* depends on the in-plane structure of the alkali-metal layer and the attendant interaction between the alkali metal and the graphite matrix. The diffuse scattering in Fig. 1 extends rod-like in the *l* direction, implying that there are no Rb–Rb correlations between the liquid layers, and the diffuse maxima in the $\langle hk \rangle$ direction are not commensurate with any graphite distances. Modulation effects are evident, however, as seen in single crystals (Parry, 1977; Rousseaux, Moret, Guerard, Lagrange & Lelaurain, 1984, 1985; Clarke *et al.*, 1979) and inferred from careful HOPG studies (Ohshima *et al.*, 1985). At the primary graphite Bragg peaks, it was also realized (Nixon & Parry, 1969; Ohshima *et al.*, 1985; Rousseaux *et al.*, 1983) that the intensities could be better fitted by including an appreciable contribution from the intercalated metal species.

It has been shown (Reiter & Moss, 1986; Moss, Reiter, Robertson, Thompson, Fan & Ohshima, 1986) that the alkali-metal contribution to the graphite Bragg peaks arises from a modulation of the two-dimensional liquid by the graphite potential, which also causes weak

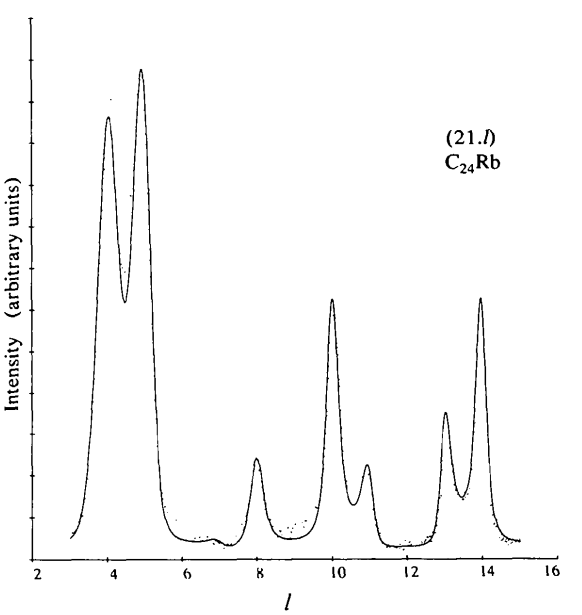

Fig. 3. (21.*l*) experimental profile. The solid line is the Hendricks–Teller fit with a projection convolution applied. The stacking-fault probability was fixed at 0·20.

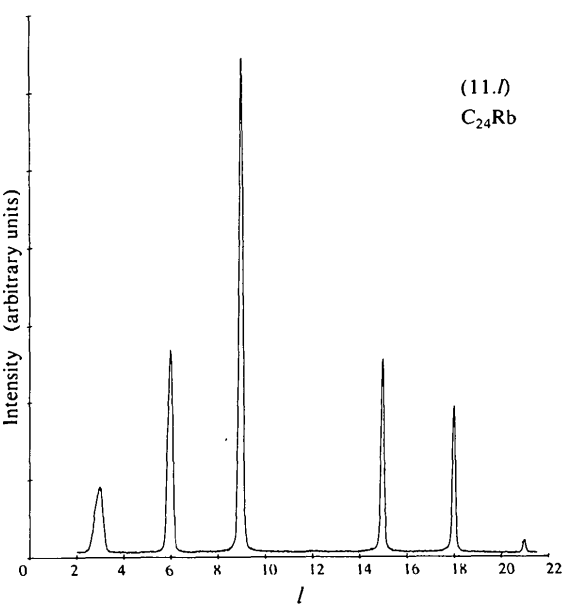

Fig. 4. (11.*l*) profiles showing peak broadening due to projection convolution. The width of the peaks follows the relation in equation (10).

Table 1. *Values of crystallographic parameters determined from* 00.*l integrated intensities (Thompson,* 1987)

c_1	x_{stoich}	B^l_C	B^l_{Rb}	R
0·2105 (1)	0·93 (3)	0·63 (6)	0·46 (14)	0·032

angular anisotropies in the liquid scattering, as seen by Clarke *et al.* (1979), Parry (1977) and Rousseaux *et al.* (1984). The effect on the scattering pattern, particularly on the Bragg peaks at the graphite reciprocal-lattice vectors $\mathbf{G}_{hk.l}$, may be calculated, and the structure factor for the Bragg-like amplitude contribution of the modulated liquid at $\mathbf{G}_{hk.l}$ is derived in detail elsewhere (Reiter & Moss, 1986). The final result for the structure factor of a single graphite–alkali–graphite sandwich for reflections other than 00.*l* is given below, where the effective modulation parameter, $\langle\rho'(\mathbf{G}_{hk})\rangle$, contributes for all *l* at constant *hk*:

$$F_{hk.l}/3 = 4f_C\exp(-M^l_C)\exp(-M^{hk}_C)\cos(\pi l c_1) \times \cos[2\pi(h + 2k)/3] + (x/6)f_{Rb}\exp(-M^l_{Rb})\langle\rho'(\mathbf{G}_{hk})\rangle. \quad (8)$$

Most of the parameters could be determined from 00.*l* analysis (Thompson, 1987) and are in Table 1. The goodness of fit, R, has been calculated as $\sum|I_{exptl} - I_{calc}|/\sum I_{exptl}$. The final unknowns include the modulation parameters $\langle\rho'(\mathbf{G}_{HK})\rangle$, which are related to the strengths of each of the (*hk*) Fourier components of the modulation potential (Reiter & Moss, 1986). We also require the in-plane Debye–Waller factor for the carbon, B^{hk}_C. (There is no in-plane rubidium Debye–Waller factor for the two-dimensional liquid.) No functional dependence of $\langle\rho'(\mathbf{G}_{hk})\rangle$ is assumed *a priori*. The value of the Fourier coefficient for each constant (*hk*) set will be determined from a fit to the scattering data along *l*.

Both of the above parameters, $\langle\rho'(\mathbf{G}_{hk})\rangle$ and B^{hk}_C, are constant at a given (*hk*). The B^{hk}_C term enters as an exponent similar to B^l_C. The value of 0·67 was taken from the work of Ohshima *et al.* (1985). While the registry model employed in that work was provisional, the extraction of a carbon Debye–Waller factor was reasonably accurate.

The parameters $\langle\rho'(\mathbf{G}_{hk})\rangle$ and x_{HT} were found through fits to the experimental profiles. The parameter $\langle\rho'(\mathbf{G}_{hk})\rangle$ enters into the expression for $|F_{hk.l}|^2$ through (8) and affects the relative intensities in (7) while the profile shapes are principally affected by the parameter x_{HT} in (6), as well as by broadening introduced by the projection on *l* of the mosaic spread of the sample.

During a scan along *l*, the mosaic spread of the reflections becomes increasingly parallel to the scan direction as *l* decreases. If the resolution element is small compared with the mosaic spread, the apparent width of the reflection will increase dramatically as *l* approaches zero. This is clearly seen in a non-stacking-fault-broadened scan such as the 11.*l* profile in Fig. 4. The projection of the radial width along *l*, due to the mosaic spread is

$$\delta_r/\sin\alpha, \quad (9)$$

where δ_r is the radial width of the peak and $\tan\alpha = q_l/q_{hk}$.

The full width at half maximum (FWHM) of non-stacking-fault-broadened peaks was fitted to

$$(\text{FWHM})^2 = (\delta_r/\sin\alpha)^2 + \Delta^2, \quad (10)$$

and δ_r was found to be 0·014 Å^{-1}, which compared well with the FWHM of the *hk*.0 peaks of 0·015 Å^{-1}. The Δ contribution, which was found to be 0·019 Å^{-1}, was included as a constant width in *l* owing to defects in staging, or to a limited correlation range (particle size) along **c*** (Kan, Misenheimer, Forster & Moss, 1987). This latter contribution to the FWHM in (10) is negligible at low *l* or in relation to the observed stacking-fault broadening in Figs. 2 or 3.

Segments of the 10.*l* profiles, which were chosen to include a zero of $F_{hk.l}$, were fitted for $\langle\rho'(\mathbf{G}_{10})\rangle$ and x_{HT} values without including projection convolution broadening. The $\langle\rho'(\mathbf{G}_{10})\rangle$ parameter was found to be 0·48 (2), and the x_{HT} varied from 3·2 to 3·4. It was expected that the x_{HT} values would vary slightly for different regions and would be slightly smaller than their true value in order to accommodate extra broadening due to the projection convolution.

The broadening due to the projection convolution is of the order of the stacking-fault broadening for the 21.*l*

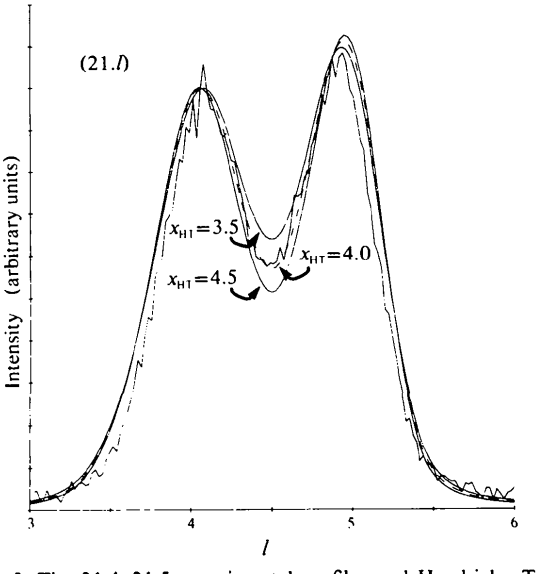

Fig. 5. The 21.4–21.5 experimental profiles and Hendricks–Teller profiles with the projection convolution applied used to estimate the true x_{HT}. The x_{HT} parameter varies from 3·5 to 4·5. It is estimated that the best fit for x_{HT}, including the projection convolution broadening, was equal to 4, which gives a stacking-fault probability of 0·20.

profiles, and therefore had a larger effect on the peak widths than in the 10.*l* profiles. The 21.4–21.5 pair, which are fairly insensitive to $\langle\rho'(\mathbf{G}_{21})\rangle$, were then used to determine x_{HT} when the convolution broadening, as calculated by (10), was applied. This is shown in Fig. 5. The x_{HT}, consistent with the x_{HT} found in the 10.*l* fits, was 4·0 (5), which converts to a stacking-fault probability of 0·20. Since the distance between centers of sandwiches is 9·04 Å, this corresponds to a coherence length of 45 Å along the *c* axis.

With this value of x_{HT}, the $\langle\rho'(\mathbf{G}_{10})\rangle$ parameter found with the partial region fits, and the convolution width calculated by (10), the total experimental 10.*l* profile could be modeled, as shown in Fig. 2. When the $\langle\rho'(\mathbf{G}_{21})\rangle$ parameter was allowed to vary, the 21.*l* profile in Fig. 3 was fit and $\langle\rho'(\mathbf{G}_{21})\rangle$ was found to be 0·04 (1).

Conclusion

A Hendricks–Teller profile analysis of the stacking-fault-broadened diffraction scans in an HOPG sample of $C_{24}Rb$ has been performed. The excellent fits which this model gives, utilizing only a second-neighbor interplanar correlation parameter, indicate that the faults are largely uncorrelated and preserve the graphite–metal–graphite sandwich. The Hendricks–Teller parameter describing the disorder in the sample was found to be 4, which corresponds to a stacking-fault probability of 0·20. By carefully applying the profile-fitting method to our data we were able to extract accurate values for the rubidium contributions to the graphite peaks in the disordered (liquid) alkali state. It has been noted that for these highly mosaic samples, caution must be taken when scanning regions parallel to the mosaic spread.

This work was supported by NSF, Grants No. DMR 82-14314 and DMR 86-03662. CT thanks the IBM Research Laboratory (Yorktown Heights, NY) for the use of their facilities under a joint study agreement. We also thank the staff at the Stanford Synchrotron Radiation Laboratory, which is supported by the Department of Energy, Office of Basic Energy Sciences, and the National Institute of Health, Biotechnology Resource Program, Division of Research Resources.

References

AXE, J. D. & HASTINGS, J. B. (1983). *Acta Cryst.* A**39**, 593–594.
BUERGER, M. J. (1960). *Crystal-Structure Analysis.* New York: John Wiley.
CLARKE, R., CASWELL, N., SOLIN, S. A. & HORN, P. M. (1979). *Phys. Rev. Lett.* **43**, 2018–2022.
CULLITY, B. D. (1956). *Elements of X-ray Diffraction.* Reading, MA: Addison-Wesley.
HASTINGS, J. B., ELLENSON, W. D. & FISCHER, J. D. (1979). *Phys. Rev. Lett.* **42**, 1552–1556.
HENDRICKS, S. & TELLER, E. (1942). *J. Chem. Phys.* **10**, 147–167.
HUSTER, M. E., HEINEY, P. A., CAJIPE, V. B. & FISCHER, J. E. (1987). *Phys. Rev. B*, **35**, 3311–3326.
KAKINOKI, J. & KOMURA, Y. (1965). *Acta Cryst.* **19**, 137–147.
KAN, X. B., MISENHEIMER, M. E., FORSTER, K. & MOSS, S. C. (1987). *Acta Cryst.* A**43**, 418–425.
KELLY, A. & GROVES, G. W. (1970). *Crystallography and Crystal Defects.* Reading, MA: Addison-Wesley.
MISENHEIMER, M. E. & ZABEL, H. (1985). *Phys. Rev. Lett.* **54**, 2521–2524.
MOORE, A. W. (1973). *Chem. Phys. Carbon*, **11**, 69–187.
MORI, M., MOSS, S. C. & JAN, Y. M. (1983). *Phys. Rev. B*, **27**, 6385–6394.
MOSS, S. C., REITER, G., ROBERTSON, J. L., THOMPSON, C., FAN, J. D. & OHSHIMA, K. (1986). *Phys. Rev. Lett.* **57**, 3191–3194.
NISHITANI, R., SUDA, K. & SUEMATSU, H. (1986). *J. Phys. Soc. Jpn*, **55**, 1601–1612.
NIXON, D. E. & PARRY, G. S. (1968). *Br. J. Appl. Phys.* **1**, 291–298.
NIXON, D. E. & PARRY, G. S. (1969). *J. Phys. C*, **2**, 1732–1741.
OHSHIMA, K., MOSS, S. C. & CLARKE, R. (1985). *Synth. Met.* **12**, 125–130.
PARRY, G. S. (1977). *Mater. Sci. Eng.* **31**, 99–106.
PARRY, G. S. & NIXON, D. E. (1967). *Nature (London)*, **216**, 909–910.
PARRY, G. S., NIXON, D. E., LESTER, K. M. & LEVENE, B. C. (1969). *J. Phys. C*, **2**, 2156–2158.
REITER, G. & MOSS, S. C. (1986). *Phys. Rev. B*, **33**, 7209–7217.
ROUSSEAUX, F., MORET, R., GUERARD, D., LAGRANGE, P. & LELAURAIN, M. (1984). *J. Phys. (Paris) Lett.* **45**, L1111–L1118.
ROUSSEAUX, F., MORET, R., GUERARD, D., LAGRANGE, P. & LELAURAIN, M. (1985). *Synth. Met.* **12**, 45–50.
ROUSSEAUX, F., TCHOUBAR, D., TCHOUBAR, C., GUERARD, D., LAGRANGE, P., HEROLD, A. & MORET, R. (1983). *Synth. Met.* **7**, 221–226.
SASAKI, S. (1984). *Anomalous Scattering Factors for Synchrotron Radiation Users, Calculated using Cromer and Liberman's Method.* Tsukuba, Japan: National Laboratory for High-Energy Physics.
THOMPSON, C. (1987). PhD Thesis, Univ. of Houston, USA.
THOMPSON, C. & MOSS, S. C. (1987). In preparation.
THOMPSON, C., MOSS, S. C., REITER, G. & MISENHEIMER, M. E. (1985). *Synth. Met.* **12**, 57–62.
WARREN, B. E. (1969). *X-ray Diffraction.* Reading, MA: Addison-Wesley.